How to cite: *Angew. Chem. Int. Ed.* **2023**, *62*, e202310880
doi.org/10.1002/anie.202310880

Block Copolymers

Precision Graphene Nanoribbon Heterojunctions by Chain-Growth Polymerization

Jin-Jiang Zhang[+], Kun Liu[+], Yao Xiao[+], Xiuling Yu, Li Huang, Hong-Jun Gao, Ji Ma, and Xinliang Feng**

Abstract: Graphene nanoribbons (GNRs) are considered promising candidates for next-generation nanoelectronics. In particular, GNR heterojunctions have received considerable attention due to their exotic topological electronic phases at the heterointerface. However, strategies for their precision synthesis remain at a nascent stage. Here, we report a novel chain-growth polymerization strategy that allows for constructing GNR heterojunction with N = 9 armchair and chevron GNRs segments (**9-AGNR/cGNR**). The synthesis involves a controlled Suzuki–Miyaura catalyst-transfer polymerization (SCTP) between 2-(6′-bromo-4,4″-ditetradecyl-[1,1′:2′,1″-terphenyl]-3′-yl) boronic ester (**M1**) and 2-(7-bromo-9,12-diphenyl-10,11-bis(4-tetradecylphenyl)-triphenylene-2-yl) boronic ester (**M2**), followed by the Scholl reaction of the obtained block copolymer (**poly-M1/M2**) with controlled M_n (18 kDa) and narrow $Đ$ (1.45). NMR and SEC analysis of **poly-M1/M2** confirm the successful block copolymerization. The solution-mediated cyclodehydrogenation of **poly-M1/M2** toward **9-AGNR/cGNR** is unambiguously validated by FT-IR, Raman, and UV/Vis spectroscopies. Moreover, we also demonstrate the on-surface formation of pristine **9-AGNR/cGNR** from the unsubstituted copolymer precursor, which is unambiguously characterized by scanning tunneling microscopy (STM).

Structurally well-defined graphene nanoribbons (GNRs) have attracted enormous interest on account of their tunable electronic properties and thus serve as promising candidates for next-generation nanoelectronics.[1–8] In the past decade, substantial progress in the bottom-up synthesis strategies towards GNRs has been achieved by utilizing either in-solution or on-surface chemistry, providing a powerful toolbox for fine-tuning their physicochemical properties.[9–18] Among them, GNR heterojunctions that combine GNRs with distinct topologies enable further electronic band structure engineering of GNRs,[19–26] which are able to bestow the resultant system with emerging topological electronic states at the interface, thus providing a completely new design space to realize exotic topological states for advanced nanoelectronics such as quantum information processing devices and spintronics.[19–20] Nevertheless, the controlled synthesis of GNR heterojunctions remains less developed due to the lack of efficient synthetic strategies. To date, the reported GNR heterojunctions have been mostly synthesized via the surface-assisted method, which relies on the co-deposition of two precursors followed by the Ullmann-type step-growth polymerization and the subsequent cyclodehydrogenation upon annealing (Figure 1a).[20–21,24–27] For example, co-deposition of 10,10′-dibromo-9,9′-bianthracene and 2,2′-di((1,1′-biphenyl)-2-yl)-10,10′-dibromo-9,9′-bianthracene leads to type I heterojunctions featuring straddling band gap;[21] besides, type II heterojunctions with staggered band gap alignment has been also realized in N-doped/undoped GNR heterojunctions.[25] Additionally, the realization of GNR heterojunctions has also been achieved by employing the iterative solution synthesis of oligomer precursor followed by surface-assisted cyclodehydrogenation with matrix-assisted direct (MAD) transfer technique. However, this labor-intensive synthetic protocol led to limitations in achieving extended lengths for GNR heterojunction.[28] Very recently, the first solution synthesis of GNR heterojunctions was demonstrated, in which block copolymer obtained from two distinct polymer segments is required to afford GNR heterojunctions by later Scholl

[*] J.-J. Zhang,[+] J. Ma, X. Feng
Max Planck Institute of Microstructure Physics
Weinberg 2, 06120 Halle (Germany)
E-mail: ji.ma@mpi-halle.mpg.de
xinliang.feng@tu-dresden.de

K. Liu,[+] X. Yu, J. Ma, X. Feng
Center for Advancing Electronics Dresden (cfaed) & Faculty of Chemistry and Food Chemistry, Technische Universität Dresden
Mommsenstrasse 4, 01062 Dresden (Germany)

Y. Xiao,[+] L. Huang, H.-J. Gao
Beijing National Center for Condensed Matter Physics and Institute of Physics, Chinese Academy of Sciences
100190 Beijing (China)

and
School of Physical Sciences, University of Chinese Academy of Sciences
100190 Beijing (China)

[+] These authors contributed equally to this work.

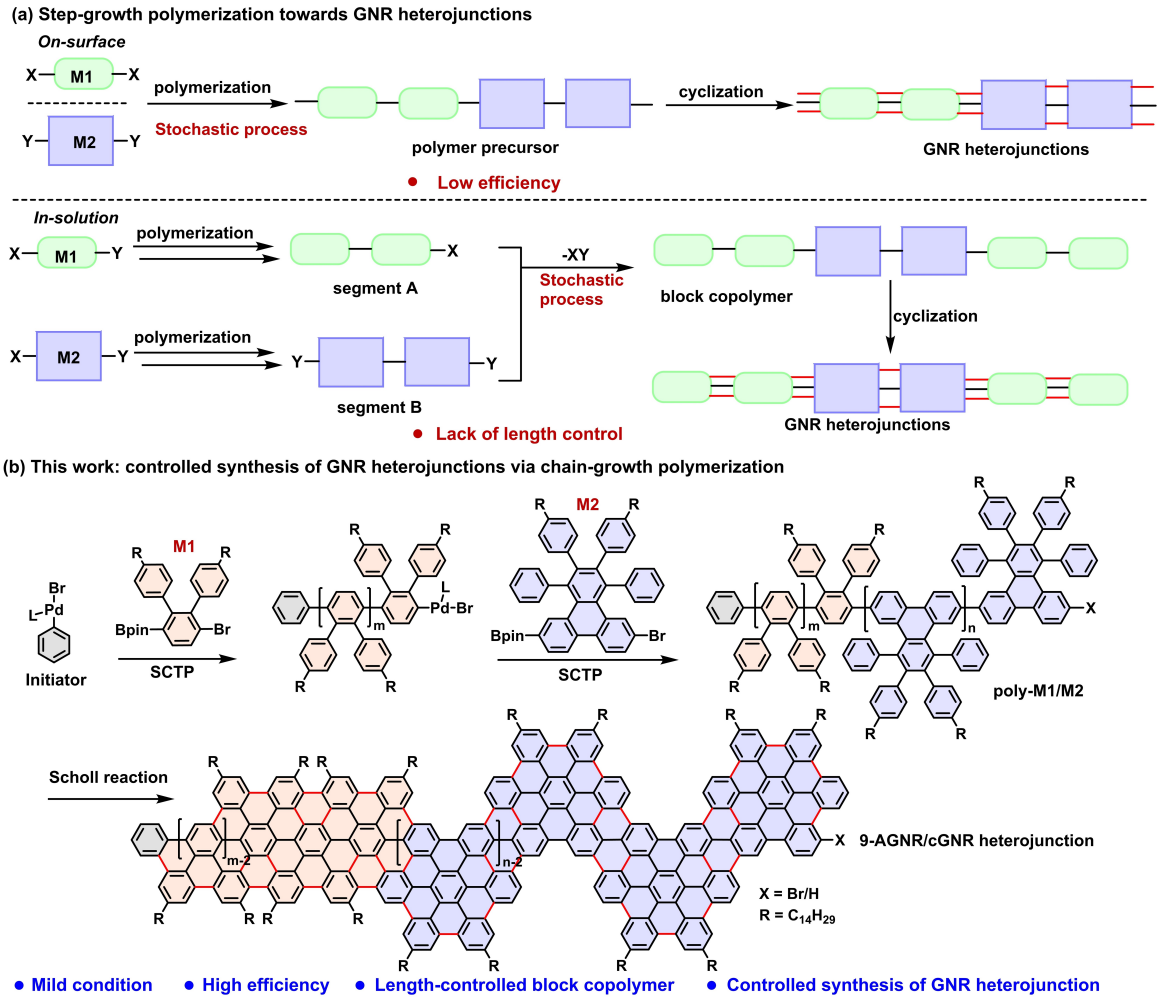

Figure 1. (a) Schematic representation of step-growth polymerization toward GNR heterojunctions. (b) Controlled synthesis of **9-AGNR/cGNR** heterojunction by employing chain-growth polymerization in current work.

reaction (Figure 1a).[29] Despite the recent developments, all the aforementioned GNR heterojunctions, either achieved by on-surface or in solution synthesis, are synthesized from the polyphenylene precursor obtained via step-growth polymerization, which results in the GNR heterojunctions being synthesized with either limited length or an uncontrollable manner. Thereby, it is highly desirable to explore the controlled synthetic strategies to efficiently construct long GNR heterojunctions.

Inspired by the modular synthesis of block copolymers via living chain-growth polymerization,[30–38] we envisioned that this approach could be applicable to prepare the precision GNR heterojunctions from pre-designed block copolymer precursors. Herein, we report the first synthesis of GNR heterojunctions (**9-AGNR/cGNR**) bearing N = 9 armchair (**9-AGNR**) and chevron GNR (**cGNR**) backbones through the chain-growth polymerization of two different monomers and subsequent cyclodehydrogenation of the obtained block polyphenylene precursor (Figure 1b). Notably, the Suzuki–Miyaura catalyst-transfer polymerization (SCTP) of 2-(6′-bromo-4,4″-ditetradecyl-[1,1′:2′,1″-terphenyl]-3′-yl) boronic ester (**M1**) and 2-(7-bromo-9,12-diphenyl-10,11-bis(4-tetradecylphenyl)-triphenylene-2-yl) boronic ester (**M2**) was applied considering its mild reaction conditions, tunable reactivity, and excellent functional group tolerance. The successful chain-growth polymerization was realized firstly by using either in situ formed Ph–Pd(Ruphos)–Br or isolated Ph–Pd(^{t}Bu$_3$P)–Br as initiator, affording corresponding **poly-M1** and **poly-M2** with controlled number average molecular weight (M_n) and narrow polydispersity index ($Đ$) (1.12–1.34). Furthermore, the living nature of this SCTP enabled the one-pot synthesis of block copolymer (**poly-M1/M2**) by sequential addition of **M1** and **M2**. Finally, intramolecular cyclodehydrogenation of **poly-M1/M2** using $FeCl_3$ as oxidant successfully gave **9-AGNR/cGNR** with high efficiency. The chemical identities of **poly-M1/M2** and **9-AGNR/cGNR** were corroborated by MALDI-TOF-MS analysis, NMR, Fourier transform infrared (FT-IR), and Raman spectroscopy, respectively. Furthermore, **9-AGNR/cGNR** without substituted alkyl chains was also demonstrated by on-surface synthesis with the MAD-transfer strategy,[28,39] which enables in situ characterization of the resultant heterojunction structure by STM.

Two bifunctional monomers **M1** and **M2** were chosen to synthesize **9-AGNR/cGNR**, considering the transformation of their respective polymers to corresponding GNR structures, **9-AGNR** and **cGNR**, have been well demonstrated in solution chemistry.[40–43] To efficiently achieve copolymer synthesis by SCTP protocol, we first optimized the polymerization conditions of **M1** with several well-known CTP catalysts as shown in Table 1. Both palladium dialkylbiarylphosphines (Pd Sphos G3 and Pd Ruphos G3) exhibited high catalytic efficiency for **M1** polymerization at monomer-to-initiator ratio ([M]/[I]) of 25 (Entry 1 and 2), providing **poly-M1** with reasonable isolated yield of 66 % and 68 %, respectively. Nevertheless, size-exclusion chromatography (SEC) traces of the polymer samples reveal that Ruphos Pd G3 could afford **poly-M1** with higher molecular weight (M_n = 13.6 kDa), which is very close to the theoretical value ($M_n^{\text{therotical}}$ = 15.5 kDa), and a narrower distribution ($Đ$ = 1.20) compared with that of Sphos Pd G3. Noted that both polymerizations were carried out with initiators prepared in situ. However, the polymerization with the use of in situ formed PhPd(^{t}Bu$_3$P)Br as initiator results in uncontrollable polymerization ($Đ$ = 1.79) albeit with high M_n (18 kDa), which could be ascribed to the low initiation speed and serious chain transfer process during the polymerization (Entry 3). For comparison, the polymerization with isolated Ph–Pd(^{t}Bu$_3$P)–Br as the catalyst was also carried out and, surprisingly, yielded **poly-M1** with controlled M_n (13.5 kDa) and narrow $Đ$ (1.21) (Entry 4). To support the chain-growth nature of this polymerization process, we examined the relationship between M_n and [M]/[I] for **poly-M1** using in situ formed Ph–Pd(Ruphos)–Br and isolated Ph–Pd(^{t}Bu$_3$P)–Br as initiator, respectively (Figure 2). Both catalyst systems showed a linear relationship between M_n and [M]/[I], with almost no change in $Đ$ (1.12–1.23) for polymers obtained at different feed ratios, manifesting that this polymerization underwent a chain-growth manner. We then investigated the controlled polymerization of monomer **M2** under these two catalytic systems by employing in situ formed Ph–Pd(Ruphos)–Br and isolated Ph–Pd(^{t}Bu$_3$P)–Br as initiator, respectively, and found that both of them were also suitable for the controlled polymerization, affording **poly-M2** with M_n of 16 kDa ($Đ$ = 1.34) for Ph–Pd(Ruphos)–Br and 12 kDa ($Đ$ = 1.32) for Ph–Pd(^{t}Bu$_3$P)–Br, respectively, when the feeding ratio was 20 (Scheme S1, S3 and Figure S1). Although both catalyst systems exhibited similar efficiencies, we chose in situ formed Ph–Pd(Ruphos)–Br for subsequent block copolymerization because of its facile preparation and the avoidance of the initiator decomposition in the isolation process.

Table 1: Screening of SCTP using **M1**.[a]

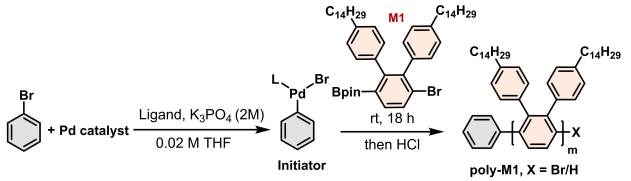

Entry	Pd Catalyst	Ligand	$[M]_0/[I]_0$	M_n (Da)[d]	$Đ$[d]	Yield[e]
1	Sphos Pd G3	Sphos	25 : 1	9.7k	1.35	66 %
2	Ruphos Pd G3	Ruphos	25 : 1	13.6k	1.20	68 %
3[b]	PhPd(^{t}Bu$_3$P)Br	tBu$_3$P	25 : 1	18k	1.79	68 %
4[c]	PhPd(^{t}Bu$_3$P)Br	/	25 : 1	13.5k	1.21	62 %
5	Ruphos Pd G3	Ruphos	15 : 1	8.9k	1.15	64 %
6	Ruphos Pd G3	Ruphos	50 : 1	22k	1.12	62 %
7	Ruphos Pd G3	Ruphos	75 : 1	30k	1.18	60 %
9	PhPd(^{t}Bu$_3$P)Br	/	15 : 1	9k	1.19	66 %
10	PhPd(^{t}Bu$_3$P)Br	/	50 : 1	21k	1.21	62 %
11	PhPd(^{t}Bu$_3$P)Br	/	75 : 1	34k	1.23	63 %

[a] Reaction conditions: **M1** (0.036 mmol, 1 equiv), Pd catalyst, Ligand, 4-bromobenzene (1 equiv. relative to the catalyst), K_3PO_4 (2 M, 10 equiv), THF. [b] PhPd(^{t}Bu$_3$P)Br is in situ formed from $Pd_2(dba)_3$, polymerization was performed under 0 °C. [c] isolated PhPd(^{t}Bu$_3$P)Br was directly used as initiator for polymerization under 0 °C. [d] Absolute molecular weight and polydispersity index were determined by SEC using a MALLS detector. [e] Isolated yield.

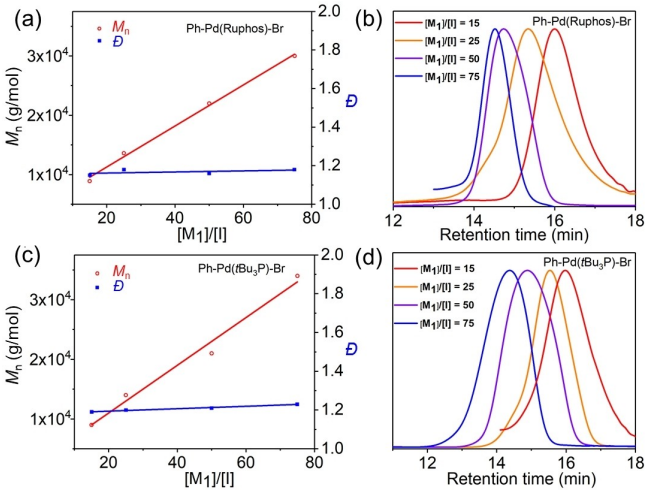

Figure 2. Plot of M_n versus [M]/[I] (a and c) and normalized SEC elution profiles (b and d) for **poly-M1** prepared by SCTP using in situ formed Ph–Pd(Ruphos)–Br and isolated Ph–Pd(^{t}Bu$_3$P)–Br as initiator, respectively. The catalyst system is noted in the panel.

For the block copolymerization of **M1** and **M2**, we polymerized **M1** firstly considering that successive catalyst-transfer polymerizations should be conducted from a monomer with lower π-donor ability to a monomer with higher π-donor ability.[37] The **poly-M1** was prepared with M_n of 8.9 kDa and narrow $Đ$ of 1.15 ([M1]/[I] = 15/1) using our optimized condition (Figure 3). After **M1** was completely consumed as indicated by NMR measurement, to the same reaction pot, **M2** was added to produce the block copolymer **poly-M1/M2** ([M2]/[I] = 15/1) (Figure 3a). SEC analysis of the copolymer clearly shifted to a higher molecular weight region (M_n = 18 kDa) albeit with a slightly broader $Đ$ (1.45), compared with that of **poly-M1** block (Figure 3b). Moreover, the ^{1}H NMR spectrum of the resulting block copolymer clearly showed featured signals of **poly-M1** (5.97–6.30 and 6.76 ppm) and **poly-M2** (7.98 and 8.26 ppm) (Figure 3c). The block ratio of **M1** to **M2** was calculated to be around 1.6 : 1 from the integration of the protons in the aromatic region, which is consistent with the ratio estimated from SEC traces analysis (1.5 : 1). Addition-

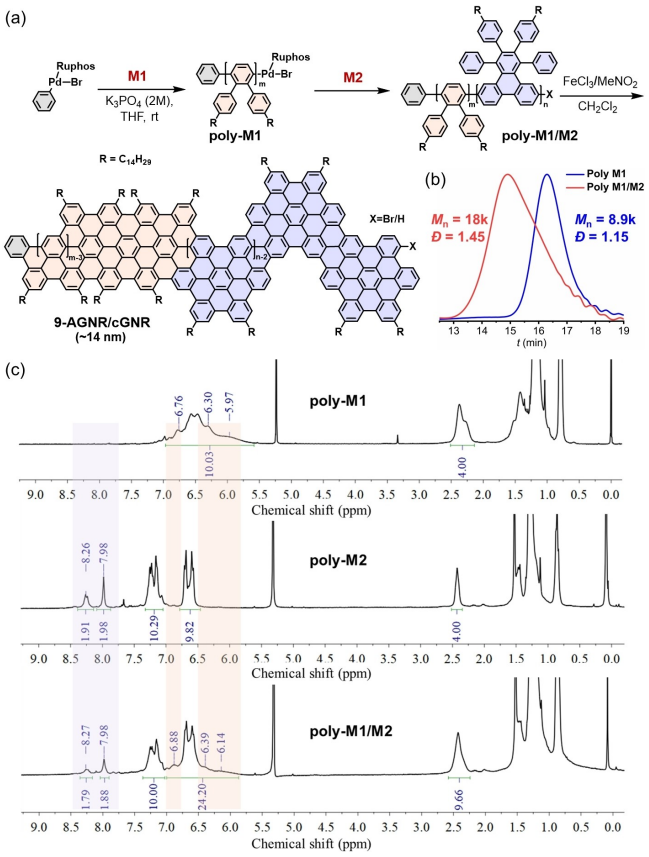

Figure 3. (a) Synthesis of **poly-M1/M2** and **9-AGNR/cGNR**. (b) SEC curves of **poly-M1** and **poly-M1/M2**, absolute molecular weight was determined by SEC analysis. (c) NMR comparison of **poly-M1**, **poly-M2** and **poly-M1/M2** (CD_2Cl_2, rt).

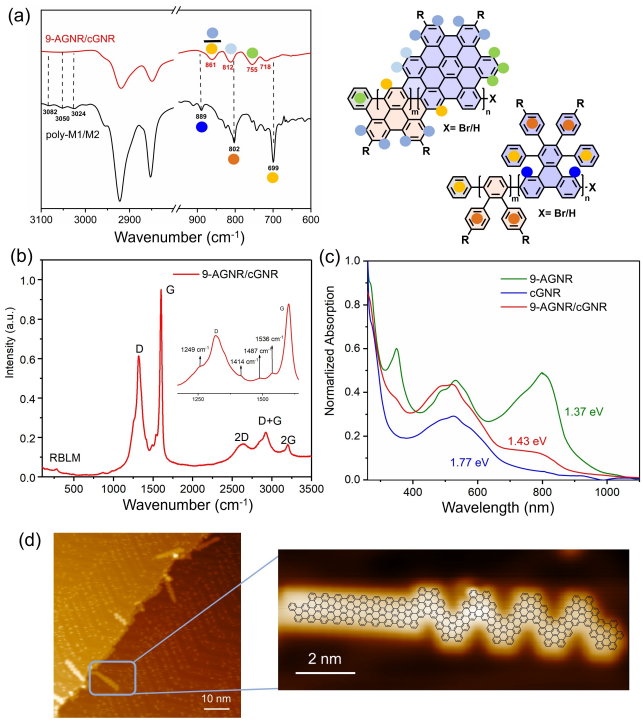

Figure 4. (a) FTIR spectra of **poly-M1/M2** and **9-AGNR/cGNR**. (b) Raman spectrum of the **9-AGNR/cGNR** measured at 532 nm. (c) UV/Vis absorption spectra of the **9-AGNR**, **cGNR** and **9-AGNR/cGNR** in NMP solution (0.1 mg mL^{-1}). (d) Large-scale (left) and zoom-in (right) topographic STM images of unsubstituted **9-AGNR/cGNR** on Au(111) (left: V_s = -1 V, I_t = 50 pA; right: V_s = -0.1 V, I_t = 50 pA).

ally, matrix-assisted laser desorption/ionization time-of-flight mass spectrometry (MALDI-TOF-MS) analysis shows a sequence of peaks with an interval of 620 or 922 *m/z*, corresponding to the repeating units in the **poly-M1/M2** backbone (Figure S2). These results verified the successful block copolymerization of **M1** and **M2**. Finally, the Scholl reaction of **poly-M1/M2** with $FeCl_3$ (7.0 equiv/H) as the Lewis acid and oxidant in CH_2Cl_2 for 3 days afforded **9-AGNR/cGNR** as a dark solid with high efficiency. The estimated length of **9-AGNR/cGNR** is ~14 nm based on SEC results for **poly-M1/M2**.

The obtained **9-AGNR/cGNR** was first characterized by FT-IR and Raman spectroscopies. FT-IR analysis of **poly-M1/M2** and **9-AGNR/cGNR** revealed the disappearance of the signal triad from aromatic C–H stretching vibrations at 3024, 3050, and 3082 cm^{-1}. Besides, out-of-plane C–H deformation bands at 699 and 802 cm^{-1}, which are typical for mono- and disubstituted benzene rings, were attenuated after graphitization. **9-AGNR/cGNR** exhibits a new emerging peak at 861 cm^{-1}, which should be assigned as SOLO mode (wagging of an isolated aromatic C–H bond neighbored by two C–C bonds) due to the formation of gulf edge and substituted armchair edge (Figure 4a), whereas the SOLO mode of **poly-M1/M2** locates at 889 cm^{-1} totally disappeared after Scholl reaction. The peaks at 812 and 755 cm^{-1} for **9-AGNR/cGNR** can be assigned as DUO (wagging of triply adjacent C–H groups) and TRIO mode (wagging of triply adjacent C–H groups), respectively.[44] The peak at 718 cm^{-1}, remains consistent in the spectra of both **9-AGNR/cGNR** and **poly-M1/M2**, which represents rocking modes of the alkyl chains.[45] These results verify the efficient conversion of block copolymer into **9-AGNR/cGNR**. The Raman spectrum of **9-AGNR/cGNR** exhibits an intense and sharp G-band peak and a broader D-band peak at 1601 and 1327 cm^{-1}, respectively, which are typical bands for the GNRs with fine "graphitized" structures (Figure 4b). Besides, two peaks at the low-energy side of the G band and two peaks around the D band, which are the characteristic peaks of **cGNR**, are also identified. Furthermore, the well-resolved signals are also observed at 2644, 2920, and 3206 cm^{-1}, which can be assigned to 2D, D+G and 2G peaks, respectively. Remarkably, a distinct peak from a ribbon width-specific low-frequency mode, namely the radial breathing like mode (RBLM), can be observed for **9-AGNR/cGNR** at 288 cm^{-1} (Figure S6), which is in good agreement with the reported RBLM mode of **cGNRs** (284 cm^{-1}).[6]

Owing to the long alkyl chains densely installed at the peripheral positions to alleviate the aggregation, the obtained **9-AGNR/cGNR** could be easily dispersed upon sonication in common organic solvents, such as THF, 1,2,4-trichlorobenzene (TCB) and *N*-methylpyrrolidone (NMP).

As shown in Figure 4c, the UV/Vis absorption spectrum of **9-AGNR/cGNR** was recorded in NMP (0.1 mg/mL) in comparison to that of **9-AGNR** and **cGNR** obtained from **poly-M1** and **poly-M2**, respectively. For **cGNR** and **9-AGNR**, the maximum longest wavelength absorption peaks are located at 526 and 800 nm, respectively, which are in good agreement with the reported cases.[40–41] The maximum longest wavelength absorption of **9-AGNR/cGNR** displays a considerable red-shift into the near-infrared (NIR) region with a broad absorption peak at ~802 nm compared with that of chevron GNR (526 nm), and it is very close to the lowest energy absorption band of **9-AGNR** (810 nm). Besides, a small band around 345 nm was observed for **9-AGNR/cGNR**, which should be attributed to the **9-AGNR** segment. The optical band gap of **9-AGNR/cGNR** is estimated to be 1.43 eV from the onset of the absorption, which is slightly larger than that of **9-AGNR** (1.37 eV) but significantly narrowed than that of **cGNR** (1.77 eV), demonstrating the ability of heterojunctions for fine-tuning the electronic structure of GNRs.

In parallel with in-solution synthesis, on-surface synthesis of **9-AGNR/cGNR** based on non-alkyl chains substituted block copolymer (**poly-M1a/M2a**) was also performed by employing MAD transfer technique, which enables in situ characterization of the heterojunction structure via STM. **Poly-M1a/M2a** was obtained with M_n of 5.2 kDa and narrow $Đ$ (1.27) when the feed ratio of [M1a]:[M2a]:[I] was 10:10:1 (Scheme S4). The successful copolymerization was also demonstrated by SEC analysis and NMR measurements (Figures S3 and S4). Subsequently, **poly-M1a/M2a** in a pyrene matrix (0.1 wt%) for MAD transfer onto a clean Au(111) surface held at room temperature (see the detailed procedure in Supporting Information). Annealing of the molecule-decorated surface at 350 K for 10 h and then 540 K for 10 min induces sublimation of the matrix. Further annealing at 630 K for 20 min induces a thermal cyclodehydrogenation that transforms the **poly-M1a/M2a** into the fully fused backbone of **9-AGNR/cGNR**. Figure 4d shows a typical constant-current STM image of resultant **9-AGNR/cGNR** on Au(111), in which the length of **9-AGNR** and **cGNR** segments matches well with the calculated value according to the degree of co-polymerization, as indicated by the superimposed chemical structure in the right image of Figure 4d.

In summary, we have demonstrated for the first time the controlled synthesis of **9-AGNR/cGNR** heterostructure from a well-designed block polyphenylene precursor via living chain-growth polymerization of two monomers. The structure of block copolymer and resultant **9-AGNR/cGNR** were comprehensively validated by NMR, FT-IR and Raman analysis. Moreover, the on-surface formation of **9-AGNR/cGNR** from unsubstituted block-copolymer was also demonstrated and further in situ characterized by STM. This work opens a door for precision synthesis of GNR heterojunctions with diverse structures. Further studies on the preparation of novel GNR heterostructures via this strategy as well as the integration of these fascinating carbon materials in advanced nanoelectronic devices are currently underway in our laboratory.

Acknowledgements

This research was financially supported by the EU Graphene Flagship (Graphene Core 3, 881603), ERC Consolidator Grant (T2DCP, 819698), H2020-MSCA-ITN (ULTIMATE, No. 813036), the Center for Advancing Electronics Dresden (cfaed), H2020-EU.1.2.2.—FET Proactive Grant (LIGHT-CAP, 101017821) and the DFG-SNSF Joint Switzerland-German Research Project (EnhanTopo, No. 429265950), and the National Natural Science Foundation of China (61888102). We thank Dr. Jinxin Liu for the Raman measurement, Dr. Yubin Fu for the helpful discussion as well as Dr. Qi Zheng and Mr. Xiaoshuai Fu for their experimental support. Open Access funding enabled and organized by Projekt DEAL.

Conflict of Interest

The authors declare no conflict of interest.

Data Availability Statement

The data that support the findings of this study are available from the corresponding author upon reasonable request.

Keywords: Block Copolymer · Chain-Growth Polymerization · Graphene Nanoribbons · Heterojunctions · Precision Synthesis

[1] R. S. K. Houtsma, J. de la Rie, M. Stohr, *Chem. Soc. Rev.* **2021**, *50*, 6541–6568.
[2] A. Narita, X. Y. Wang, X. Feng, K. Müllen, *Chem. Soc. Rev.* **2015**, *44*, 6616–6643.
[3] H. Wang, H. S. Wang, C. Ma, L. Chen, C. Jiang, C. Chen, X. Xie, A.-P. Li, X. Wang, *Nat. Rev. Phys.* **2021**, *3*, 791–802.
[4] G. Z. Magda, X. Jin, I. Hagymasi, P. Vancso, Z. Osvath, P. Nemes-Incze, C. Hwang, L. P. Biro, L. Tapaszto, *Nature* **2014**, *514*, 608–611.
[5] W. Niu, S. Sopp, A. Lodi, A. Gee, F. Kong, T. Pei, P. Gehring, J. Nagele, C. S. Lau, J. Ma, J. Liu, A. Narita, J. Mol, M. Burghard, K. Müllen, Y. Mai, X. Feng, L. Bogani, *Nat. Mater.* **2023**, *22*, 180–185.
[6] R. Sainz, M. Del Pozo, M. Vilas-Varela, J. Castro-Esteban, M. Perez Corral, L. Vazquez, E. Blanco, D. Pena, J. A. Martin-Gago, G. J. Ellis, M. D. Petit-Dominguez, C. Quintana, E. Casero, *Sci. Rep.* **2020**, *10*, 14614.
[7] C. Tian, W. Miao, L. Zhao, J. Wang, *Rev. Phys.* **2023**, *10*, 100082.
[8] V. Saraswat, R. M. Jacobberger, M. S. Arnold, *ACS Nano* **2021**, *15*, 3674–3708.
[9] W. Niu, J. Ma, X. Feng, *Acc. Chem. Res.* **2022**, *55*, 3322–3333.
[10] M. Shekhirev, A. Sinitskii, *Phys. Sci. Rev.* **2017**, *2*, https://doi.org/10.1515/psr-2016–0108.
[11] Y. Yano, N. Mitoma, H. Ito, K. Itami, *J. Org. Chem.* **2020**, *85*, 4–33.
[12] J. J. Zhang, J. Ma, X. Feng, *Macromol. Chem. Phys.* **2023**, *224*, 2200232.
[13] A. Jolly, D. Miao, M. Daigle, J. F. Morin, *Angew. Chem. Int. Ed.* **2020**, *59*, 4624–4633.
[14] X. Zhou, G. Yu, *Adv. Mater.* **2020**, *32*, 1905957.

[15] Z. Chen, A. Narita, K. Müllen, *Adv. Mater.* **2020**, *32*, 2001893.
[16] D. G. de Oteyza, A. Garcia-Lekue, M. Vilas-Varela, N. Merino-Diez, E. Carbonell-Sanroma, M. Corso, G. Vasseur, C. Rogero, E. Guitian, J. I. Pascual, J. E. Ortega, Y. Wakayama, D. Pena, *ACS Nano* **2016**, *10*, 9000–9008.
[17] R. K. Dubey, M. Melle-Franco, A. Mateo-Alonso, *J. Am. Chem. Soc.* **2021**, *143*, 6593–6600.
[18] J. Li, S. Sanz, N. Merino-Diez, M. Vilas-Varela, A. Garcia-Lekue, M. Corso, D. G. de Oteyza, T. Frederiksen, D. Pena, J. I. Pascual, *Nat. Commun.* **2021**, *12*, 5538.
[19] D. J. Rizzo, G. Veber, T. Cao, C. Bronner, T. Chen, F. Zhao, H. Rodriguez, S. G. Louie, M. F. Crommie, F. R. Fischer, *Nature* **2018**, *560*, 204–208.
[20] O. Gröning, S. Wang, X. Yao, C. A. Pignedoli, G. Borin Barin, C. Daniels, A. Cupo, V. Meunier, X. Feng, A. Narita, K. Müllen, P. Ruffieux, R. Fasel, *Nature* **2018**, *560*, 209–213.
[21] Y. C. Chen, T. Cao, C. Chen, Z. Pedramrazi, D. Haberer, D. G. de Oteyza, F. R. Fischer, S. G. Louie, M. F. Crommie, *Nat. Nanotechnol.* **2015**, *10*, 156–160.
[22] G. D. Nguyen, H. Z. Tsai, A. A. Omrani, T. Marangoni, M. Wu, D. J. Rizzo, G. F. Rodgers, R. R. Cloke, R. A. Durr, Y. Sakai, F. Liou, A. S. Aikawa, J. R. Chelikowsky, S. G. Louie, F. R. Fischer, M. F. Crommie, *Nat. Nanotechnol.* **2017**, *12*, 1077–1082.
[23] B. V. Senkovskiy, A. V. Nenashev, S. K. Alavi, Y. Falke, M. Hell, P. Bampoulis, D. V. Rybkovskiy, D. Y. Usachov, A. V. Fedorov, A. I. Chernov, F. Gebhard, K. Meerholz, D. Hertel, M. Arita, T. Okuda, K. Miyamoto, K. Shimada, F. R. Fischer, T. Michely, S. D. Baranovskii, K. Lindfors, T. Szkopek, A. Gruneis, *Nat. Commun.* **2021**, *12*, 2542.
[24] P. S. Costa, J. D. Teeter, A. Enders, A. Sinitskii, *Carbon* **2018**, *134*, 310–315.
[25] J. Cai, C. A. Pignedoli, L. Talirz, P. Ruffieux, H. Sode, L. Liang, V. Meunier, R. Berger, R. Li, X. Feng, K. Mullen, R. Fasel, *Nat. Nanotechnol.* **2014**, *9*, 896–900.
[26] C. Bronner, R. A. Durr, D. J. Rizzo, Y. L. Lee, T. Marangoni, A. M. Kalayjian, H. Rodriguez, W. Zhao, S. G. Louie, F. R. Fischer, M. F. Crommie, *ACS Nano* **2018**, *12*, 2193–2200.
[27] C. Dobner, G. Li, M. Sarker, A. Sinitskii, A. Enders, *RSC Adv.* **2022**, *12*, 6615–6618.
[28] J. Yin, P. H. Jacobse, D. Pyle, Z. Wang, M. F. Crommie, G. Dong, *J. Am. Chem. Soc.* **2022**, *144*, 16012–16019.
[29] X. Zhang, Y. Hu, C. R. Lien-Medrano, J. Li, J. Shi, X. Qin, Z. Liao, Y. Wang, Z. Wang, J. Li, J. Chen, G. Zhang, J. V. Barth, T. Frauenheim, W. Auwarter, A. Narita, K. Müllen, C. A. Palma, *J. Am. Chem. Soc.* **2023**, *145*, 8757–8763.
[30] T. Yokozawa, Y. Ohta, *Chem. Rev.* **2016**, *116*, 1950–1968.
[31] K. B. Seo, I. H. Lee, J. Lee, I. Choi, T. L. Choi, *J. Am. Chem. Soc.* **2018**, *140*, 4335–4343.
[32] J. Lee, H. Kim, H. Park, T. Kim, S. H. Hwang, D. Seo, T. D. Chung, T. L. Choi, *J. Am. Chem. Soc.* **2021**, *143*, 11180–11190.
[33] H. H. Zhang, C. H. Xing, Q. S. Hu, *J. Am. Chem. Soc.* **2012**, *134*, 13156–13159.
[34] H. Kim, J. Lee, T. Kim, M. Cho, T. L. Choi, *Angew. Chem. Int. Ed.* **2022**, *61*, e202205828.
[35] M. V. Bautista, A. J. Varni, J. Ayuso-Carrillo, M. C. Carson, K. J. T. Noonan, *Polym. Chem.* **2021**, *12*, 1404–1414.
[36] S. von Kugelgen, I. Piskun, J. H. Griffin, C. T. Eckdahl, N. N. Jarenwattananon, F. R. Fischer, *J. Am. Chem. Soc.* **2019**, *141*, 11050–11058.
[37] H.-H. Zhang, Y.-X. Zhu, W. Wang, J. Zhu, P. V. Bonnesen, K. Hong, *Polym. Chem.* **2018**, *9*, 3342–3346.
[38] M. V. Bautista, A. J. Varni, J. Ayuso-Carrillo, C. H. Tsai, K. J. T. Noonan, *ACS Macro Lett.* **2020**, *9*, 1357–1362.
[39] R. D. McCurdy, P. H. Jacobse, I. Piskun, G. C. Veber, D. J. Rizzo, R. Zuzak, Z. Mutlu, J. Bokor, M. F. Crommie, F. R. Fischer, *J. Am. Chem. Soc.* **2021**, *143*, 4174–4178.
[40] G. Li, K. Y. Yoon, X. Zhong, X. Zhu, G. Dong, *Chem. Eur. J.* **2016**, *22*, 9116–9120.
[41] T. H. Vo, M. Shekhirev, D. A. Kunkel, M. D. Morton, E. Berglund, L. Kong, P. M. Wilson, P. A. Dowben, A. Enders, A. Sinitskii, *Nat. Commun.* **2014**, *5*, 3189.
[42] T. H. Vo, M. Shekhirev, A. Lipatov, R. A. Korlacki, A. Sinitskii, *Faraday Discuss.* **2014**, *173*, 105–113.
[43] T. H. Vo, M. Shekhirev, D. A. Kunkel, F. Orange, M. J. Guinel, A. Enders, A. Sinitskii, *Chem. Commun.* **2014**, *50*, 4172–4174.
[44] M. Tommasini, A. Lucotti, M. Alfe, A. Ciajolo, G. Zerbi, *Spectrochim. Acta Part A* **2016**, *152*, 134–148.
[45] B. Yang, Y. Gu, G. M. Paterno, J. Teyssandier, A. Maghsoumi, A. J. Barker, K. S. Mali, F. Scotognella, S. De Feyter, M. Tommasini, X. Feng, A. Narita, K. Müllen, *Chem. Eur. J.* **2023**, *29*, e202203981.

Manuscript received: July 28, 2023
Accepted manuscript online: August 18, 2023
Version of record online: September 6, 2023